Three Distinct Inner Dynein Arms in *Chlamydomonas* Flagella: Molecular Composition and Location in the Axoneme

Gianni Piperno, Zenta Ramanis, Elizabeth F. Smith,* and Winfield S. Sale*

The Rockefeller University, New York 10021; and * Department of Anatomy and Cell Biology, Emory University School of Medicine, Atlanta, Georgia 30322

Abstract. The molecular composition and organization of the row of axonemal inner dynein arms were investigated by biochemical and electron microscopic analyses of *Chlamydomonas* wild-type and mutant axonemes. Three inner arm structures could be distinguished on the basis of their molecular composition and position in the axoneme as determined by analysis of *pf*30 and *pf*23 mutants. The three inner arm structures repeat every 96 nm and are referred to here as inner arms I1, I2, and I3. I1 is proximal to the radial spoke S1, whereas I2 and I3 are distal to spokes S1 and S2, respectively. The mutant *pf*30 lacks I1 whereas the mutant *pf*23 lacks both I1 and I2 but has a normal inner arm I3. Each of the six heavy chains that was identified as an inner dynein arm subunit has a site for ATP binding and hydrolysis. Two of the heavy chains together with a polypeptide of 140,000 molecular weight form the inner arm I1 and were extracted from the axoneme as a complex that had a sedimentation coefficient close to 21S at high ionic strength. Different subsets of two of the remaining four heavy chains form the inner arms I2 and I3. These arms at high ionic strength are dissociated as 11S particles that include one heavy chain, one intermediate chain, two light chains, and actin. These and other lines of evidence indicate that the inner arm I1 is different in structure and function from the inner arms I2 and I3.

THE inner dynein arms, unlike the outer dynein arms, are both necessary and sufficient to generate ciliary and flagellar axonemal bending (4). However, the molecular organization and composition of the inner dynein arms are not as well understood as those of the outer row of arms (for review see references 8, 16, 17, and 25). Through biochemical and electron microscopic analyses of *Chlamydomonas* wild-type and mutant axonemes, here we have begun to determine the composition of each inner dynein arm. In addition, we demonstrate that the row of inner arms is formed by three distinct structures, each having a specific location relative to the radial spokes S1 and S2 (see references 7 and 8).

Several lines of evidence have suggested that the row of inner dynein arms is formed by more than one type of structure. First, as many as five inner arm heavy chains were identified by combined biochemical and microscopic analysis of *Chlamydomonas* mutants lacking either outer or inner dynein arms (11). Therefore, the existence of multiple inner arms was implied, as all dynein arms characterized so far are formed by at most three heavy chain subunits (6, 28). Second, in contrast to mutations affecting outer arm assembly, which cause the loss of all outer arm heavy chains along with the outer arms (15), mutations known to affect the assembly of inner arms cause the lack of only a subset of inner arm heavy chains (4, 20). Third, EM of quick-frozen and deep-etched samples has revealed that there are two types of inner arm structures, referred to as dyads and triads organized in triad-dyad-dyad triplet groups which repeat with a 96-nm interval (7, 8). Together, these data suggest that the inner dynein arms, unlike the outer dynein arms, are heterogeneous in structure and composition.

To further investigate this hypothesis of inner dynein arm organization, we have adopted new electrophoretic conditions for separation of inner arm heavy chains and then reexamined inner arm deficient mutants described previously (4, 11, 20). We have also analyzed those same mutants by EM of longitudinal sections. Through these combined analyses we have determined the location of three specific types of inner arms in the axoneme and begun to investigate their function.

Materials and Methods

Strains and Culture of Chlamydomonas Cells

The strain 137c, mating type +, was adopted as wild type. The mutants analyzed in this study are listed in Table I. recombinant strains *pf*30*pf*28, *pf*14*pf*28, and *pf*18*pf*28 were selected from nonparental ditype tetrads, whereas *pf*23*pf*28 was selected from a tetratype tetrad. Cells from each recombinant strain have short (approximately half of the normal length or less), paralyzed flagella. 4-d cultures and ^{35}S-labeling of cells were performed on solid medium containing 25 mCi/liter of [^{35}S]sulfuric acid (18).

Preparation of Flagella, Axonemes, and Axonemal Fractions

Flagella were severed from cell bodies by the pH shock method and isolated by differential centrifugation (11). To prepare axonemes, a stock solution of

Table I. Chlamydomonas Mutant Strains

Strain	Flagellar phenotype	Linkage group of defective gene	Missing structure in the axoneme	Reference
*pf*28(*oda*2)*	Abnormal motion	XI	Outer arms	15, 19
*oda*1	Abnormal motion		Outer arms	15
*oda*6	Abnormal motion	XII	Outer arms	15
*pf*13A	Short flagella paralyzed	IX	Outer arms	11
*pf*14	Occasional slow motion	XII	Radial spokes	12
*pf*18	Occasional slow motion	II	Central complex	1
*pf*23	Short flagella paralyzed	XI	Outer and inner arm deficiency	11
*pf*30(*ida*)*	Abnormal motion	XII	inner arm deficiency	4, 16

* In parentheses, denomination of alleles that were isolated in a different laboratory.

NP-40 was added to suspensions of flagella to the final concentration of 0.1% before the final centrifugation. Extracts enriched in inner dynein heavy chains were prepared from *pf*28 axonemes by exposure to 0.5 M NaCl, 1 mM ATP, 4 mM $MgCl_2$, 1 mM DTT, and 10 mM Hepes (pH 7.2) (22). Determination of protein concentrations and radioactivity were as described (21). For certain electron microscopic experiments, flagella were isolated by the dibucaine method (29). Flagella prepared by the dibucaine or the pH shock method appeared identical in structure and composition.

Photocleavage of Dynein Heavy Chains

^{35}S-labeled extracts of *pf*28 axonemes containing dynein heavy chains, (~0.5 ml, 1 mg/ml of protein, 100,000 cpm/μg) were dialyzed against 0.45 M Na acetate, 2.5 mM Mg acetate, 0.5 mM EDTA, and 0.1 mM PMSF, 10 mM Hepes (pH 7.5). After dialysis, ATP and Na_3VO_4 were added to final concentrations of 50 and 2 μM, respectively. Irradiation of samples was performed as described by Gibbons and Gibbons (5).

Electrophoresis and Densitometry of Autoradiograms

Electrophoresis of dynein heavy chains was performed essentially as described by Piperno (20). However, the following modifications were introduced to improve the resolution of inner dynein arm heavy chains. We used a discontinuous slab gel composed of a 3.2% polyacrylamide stacking layer and a 3.6–5% polyacrylamide resolving layer. The slab did not contain urea. Ultra pure acrylamide from International Biotechnologies, Inc. (New Haven, CT) and sodium dodecyl sulfate 99.0% pure from BDH Laboratories (Poole, UK) were used for the preparation of gels.

These new conditions led to the resolution of six electrophoretic bands each containing at least one inner dynein arm heavy chain from *pf*28 axonemes (Fig. 1). In contrast, polypeptides I, II, and V of wild-type axonemes, the α, β, and γ heavy chains, respectively of outer dynein arms (22), were not resolved from each other and from polypeptides III and IV of the inner dynein arms. Instead they formed two electrophoretic bands (Fig. 1, first lane [also see Fig. 1, reference 20). Under these new electrophoretic conditions, polypeptides I, II, and III compose the slowest major band, whereas polypeptides IV and V compose the second major band. The electrophoretic mobilities of these components were determined by comparing the electrophoretic patterns formed by axonemal polypeptides of the mutants *pf*28, *pf*30, and the recombinant strain *pf*28*pf*30. *pf*28 and *pf*30 lack polypeptides I, II, and V, and III and IV, respectively (20). Therefore, using the new conditions of gel electrophoresis it was possible to identify polypeptides III and IV as defined under the previous conditions of gel electrophoresis. In contrast, it was not possible to identify which of the remaining four bands, formed by *pf*28 inner arm heavy chains under the new conditions of electrophoresis, corresponded to inner arm electrophoretic components VI, and VII, and VIII as defined previously (11, 24).

Densitometry of autoradiograms was performed with a video densitometer (model 620; Bio-Rad Laboratories, Richmond, CA). Quantitative measurements were performed in the range of linear response of autoradiograms of gels produced by exposure for an appropriate length of time. 1D Analyst Software (Bio-Rad Laboratories) was used to determine relative optical density of each electrophoretic band.

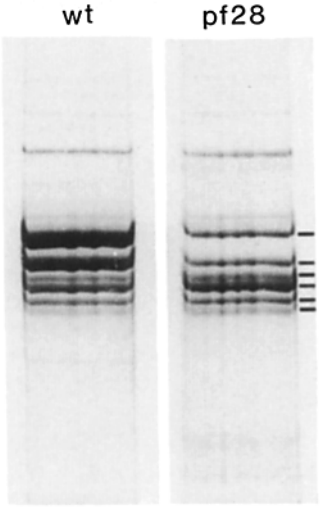

Figure 1. Electrophoretograms of ^{35}S-labeled axonemal polypeptides of wild-type and *pf*28 mutant cells. Equal amounts of radioactivity were analyzed. Each panel is part of an autoradiogram containing the pattern of bands formed by dynein arm heavy chains. (*Left*) The two intense upper bands are formed by both outer and inner arm heavy chains. (*Right*) The six bands indicated by lines are formed by inner arm heavy chains.

Electron Microscopy

For structural study, isolated axonemes were sedimented at 10,000 *g*, and pellets were fixed with 1% glutaraldehyde and 1% tannic acid in a buffer containing sodium cacodylate as described previously (11). Specimens were postfixed in osmium tetroxide, dehydrated in a graded series of ethanol, and embedded in Medcast-Araldite resin (Ted Pella, Inc., Tustin, CA). 40–50 nm-thick uniform silver-gray sections were mounted on formvar coated, carbon stabilized copper grids, stained with uranyl acetate and Reynolds lead citrate, and examined at 80 kV in the JEOL 100 CX electron microscope (JEOL USA, Peabody, MA). Transverse and longitudinal sections of axonemes of wild-type and mutant cells were randomly selected and compared from more than one experiment for each cell type.

Nomenclature

New information concerning the organization of the row of inner dynein arms and the molecular composition of each arm is reported in the following section. On the basis of these data, we have adopted a new nomenclature to indicate each inner dynein arm and each heavy chain subunit that we have identified. This nomenclature reflects our present understanding of the inner dynein arm structures. However, it is not yet definitive because we have limited information on differences of primary structures and/or modifications existing among the inner dynein arm heavy chains.

Three distinct inner dynein arm structures are referred to as I1, I2, and I3, in the order of their position relative to the radial spokes. The inner arms I1 and I2 are proximal to the radial spoke S1 and S2, respectively, whereas I3 is distal to S2.

The denomination of each inner dynein heavy chain includes a number and a Greek letter or a prime. The number refers to the inner arm that contains the heavy chains. The Greek letters refer to polypeptides that are associated in 1:1 ratio, are not labeled by ^{32}P in vivo (24) and may differ in their primary structure. The prime refers to polypeptides that form a minor satellite band in motile and long flagella. Thus, as described below, the inner

dynein arm I1 is formed by the heavy chains 1α and 1β, whereas the inner arms I2 and I3 are formed by the heavy chains 2′ and 2 and 3 and 3′, respectively. The inner arm heavy chains 1α and 1β are the polypeptides formerly indicated as components III and IV (22). The heavy chains 2′, 2, 3, and 3′ formed the components formerly indicated as VI, VII, and VIII, which were found to be phosphorylated *in vivo* (24).

Until specific reagents are developed (e.g., monospecific antibodies) to identify each inner arm heavy chain, it will be necessary to use axonemes from the recombinant strains *pf*30*pf*28 and *pf*23*pf*28 as standards for the electrophoretic analysis of inner arm heavy chains. It will be shown in the following section that the recombinant strains *pf*30*pf*28 and *pf*23*pf*28 lack the dynein arm heavy chains forming the inner arm I1 and I1 and I2, respectively, as well as the outer dynein arms.

Results

Molecular Composition and Heterogeneity of Inner Dynein Arms

We began our analysis of the molecular composition of the inner dynein arms, and putative heterogeneity of those components, by focusing on the resolution of dynein heavy chain subunits of the motile outer dynein-less mutant *pf*28 (19). We resolved inner arm heavy chains of *pf*28 axonemes into six electrophoretic bands using the new electrophoretic conditions described in Materials and Methods (Fig. 1, second lane). Under the same conditions outer and inner dynein arm heavy chains of wild-type axonemes are resolved into six electrophoretic bands instead of eight, as illustrated in Fig. 1 (first lane). In *pf*28, the upper two bands have approximately the same intensity, whereas the lower four bands differ in intensity. The patterns of the four lower bands are identical in both lanes, therefore they may be formed uniquely by inner arm heavy chains.

Additional lines of evidence as described below confirm that the six bands shown in Fig. 1 (second lane) were formed by the inner arm heavy chains. First, these polypeptides were extracted in the presence of 0.5 M NaCl, ATP, and Mg^{2+}. Second, each of the six polypeptides was isolated or partially purified in association with intermediate and light chains that had previously been identified as inner dynein arm components (11, 20, 24). Finally, the same six polypeptides were specifically photocleaved by UV irradiation in the presence of ATP, Mg^{2+}, and vanadate (6).

Salt extracts from *pf*28 axonemes were prepared and aliquots were irradiated at 365 nm as described in Materials and Methods. Samples from untreated and irradiated extracts were then sedimented in a 5–20% sucrose gradient

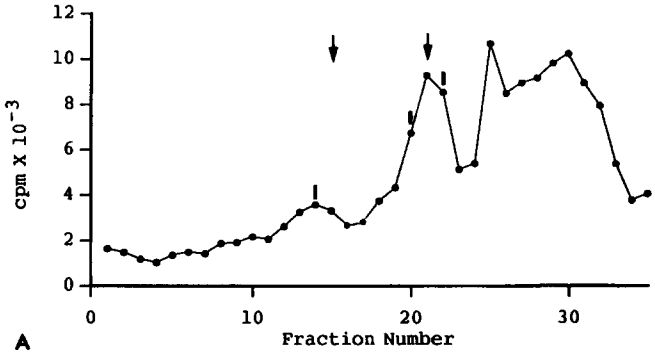

Figure 2. Sucrose gradients sedimentation profile and electrophoretograms of ^{35}S-labeled polypeptides contained in a nonirradiated salt extract from *pf*28 axonemes. (*A*) Sedimentation profile of ^{35}S-labeled proteins (load ~9.4 × 10^6 cpm, radioactivity was counted on 5-μl aliquots from each fraction). The direction of sedimentation was from right to left. Centrifugation of a 5–20% sucrose gradient in 0.5 M NaCl, 10 mM Tris-Cl (pH 7.4) was performed in a rotor (model SW55; Beckman Instruments, Inc., Palo Alto, CA) at 35,000 rpm for 10 h at 5°C. Bovine catalase (11S) and thyroglobulin (19S) were used as sedimentation standards in a parallel gradient. The positions of their sedimentation peaks are indicated by arrows. Vertical lines indicate peak fractions 14, 20, and 22 that were analyzed further. (*B*) Electrophoretograms of all polypeptides contained in fractions 9–26. Electrophoresis was performed in a discontinuous (20) 4–11% polyacrylamide gradient gel of reduced size (6 cm long, 20 cm wide, and 0.075 cm thick) at constant 20 mA. *Arrowheads* indicate intermediate and light chains cosedimenting with inner arm heavy chains. Apparent molecular weights are indicated at the right side.

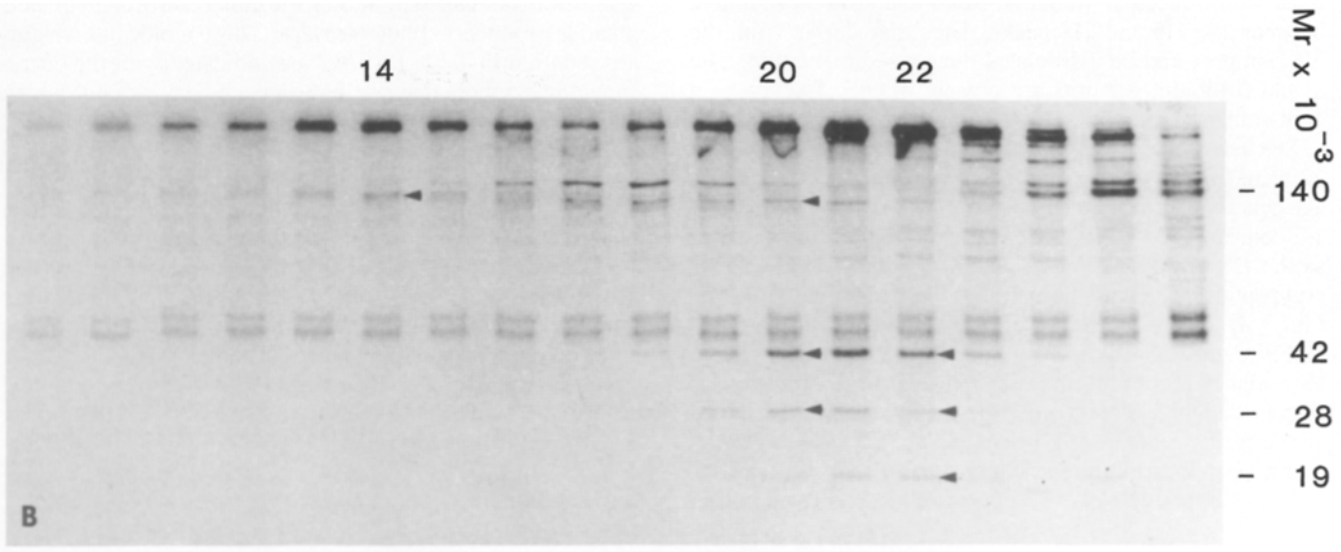

Table II. Molecular Components of Complexes Derived from Inner Dynein Arms

		11S	
	21S	Fast*	Slow*
Heavy chains‡	433 (●)	402 (■)	402
	418 (○)		399 (□)
		398 (▼)	398 (▼)
		386 (▽)	386 (▽)
Intermediate chains	140	133	
		Actin	Actin
Light chains		28	28
			19

Each polypeptide subunit is identified by its apparent molecular weight $\times 10^{-3}$ with the exception of the actin. An estimate of the molecular weight of each heavy chain was obtained by adding the molecular weight values of their putative photocleavage products.

* Differences in the composition of 11S complexes were detected by the analysis of fast and slow sides of the 11S peak.

‡ As in Fig. 3 *A*, each heavy chain, which appeared to be photocleaved, is indicated by a different symbol (*open* and *closed circles*, *squares*, and *triangles*).

containing 0.5 M NaCl. Profiles of sedimentation peaks obtained with an untreated extract are shown in Fig. 2 *A*. A major and minor peak with sedimentation coefficients of ~11S and 21S were resolved. Components of the irradiated salt extract sedimented like those of the untreated extract (not shown).

The polypeptide components of fractions 9–26 were then resolved by electrophoresis (Fig. 2 *B*). The minor 21S peak is formed by dynein heavy chains and a polypeptide of 140,000 molecular weight. The major 11S peak is formed by dynein heavy chains, a polypeptide of 133,000 molecular weight, actin and two light chains of 28,000 and 19,000 molecular weight. The distribution of the intermediate and light chains in the 11S peaks is asymmetric: the 133,000 and 19,000 components are enriched in the faster and slower regions of the peak, respectively. A summary of the polypeptides forming the two sedimentation peaks is reported in Table II. On the basis of their apparent molecular weights and with the exception of the 133,000 component, each of these polypeptides is identical to inner arm subunits described in previous studies (reviewed in reference 17). Two polypeptides with molecular weight 155,000 and 131,000 sediment between the 11S and 21S peaks. They may derive from the 21S complex and be dissociated during sedimentation. The α and β tubulin subunits are present in each fraction as a contaminant.

The heavy chain components of peak fractions 14, 20, and 22 were further resolved by electrophoresis in low percentage gels as described above (Fig. 3 *A*). The 21S peak, fraction 14, contains two high molecular weight polypeptides, whereas the 11S peak, fraction 20 and 22, contains three or four polypeptides which are partially resolved (*lines* and *symbols*, Fig. 3 *A*). The 21S heavy chains are characterized by lower mobility and equal intensity, whereas the 11S heavy chains have higher mobilities and differ in intensity. These results suggest that the 21S component is a complex containing equal amounts of two inner arm heavy chains and the 11S peak is a heterogeneous mixture of inner dynein arm subunits.

As mentioned above, the six polypeptides indicated in Fig. 3 *A* were identified as dynein heavy chains also on the basis of their sensitivity to UV-induced photocleavage performed in the presence of ATP, Mg^{2+}, and vanadate. Nonirradiated and irradiated salt extracts were sedimented through identical sucrose gradients. Photocleavage was detected by comparing autoradiograms of gels in which equal amounts of radioactivity were analyzed from fractions 14, 20, and 22 from those sucrose gradients, Fig. 3 *A*. The asterisks distinguish those samples containing polypeptides that were subjected to photocleavage. Each of the six electrophoretic bands was reduced in intensity after photocleavage although the reduction was not uniform for each component.

The occurrence of different extents of photocleavage for each of the six components under investigation is also shown by the electrophoretograms of cleavage products, which are present in fractions 14*, 20*, and 22*, Fig. 3 *B*. The relative amount of each cleavage product in those fractions can be estimated because the ^{35}S uniformly labels each heavy chain. In fact, the levels of intensity of heavy chains and cleavage products in the autoradiograms are similar to those that are revealed by silver staining in the gels (not shown).

We tentatively identified the fragments generated from each heavy chain by comparison of the intensity of heavy chain bands with intensities and distributions of cleavage products. For example, the first heavy chain characterized by the lowest electrophoretic mobility is cleaved less than the second heavy chain (Figs. 3 *A*, lanes *14* and *14**). Therefore, it may generate the two fragments that form bands of lower intensity (Fig. 3 *B*, lanes *14* and *14**, indicated by *closed circles*). The same logic, based on the evaluation of band intensity, was followed to match five additional sets of heavy chain precursor and cleavage products. A different symbol was adopted for each set of heavy chain and cleavage fragments (Fig. 3, *A* and *B*, paired fractions 14, 14*, 20, 20*, and 22, 22*).

Each heavy chain produced a large fragment of ~250,000 molecular weight and the fifth and sixth heavy chains apparently generated two large fragments that were not resolved by electrophoresis (Fig. 3 *B*, fractions 20* and 22*, *open* and *closed triangles*). The fifth and sixth heavy chains, as described below, also appeared to be interconvertible by posttranslational modification.

The apparent molecular weight of each of the six heavy chains was calculated by adding the molecular weight of their putative products of photocleavage. These molecular weights are reported in Table II. They are indicated with the corresponding symbols that distinguish each heavy chain, which appeared to be photocleaved.

The evidence described thus far suggests the existence of six heavy chains which compose the inner row of dynein arms. The evidence also suggests that there are at least two forms of inner arms; one form composed of the two heavy chains sedimenting as a 21S complex, the other form or forms composed of the remaining four heavy chains. These four polypeptides either have different primary structures and derive from separate subsets of inner dynein arms or have the same primary structures and derive from identical inner arms. In this case, they are resolved by gel electrophoresis because they are modified posttranslationally. To further investigate these points we analyzed other outer and inner dynein defective mutants.

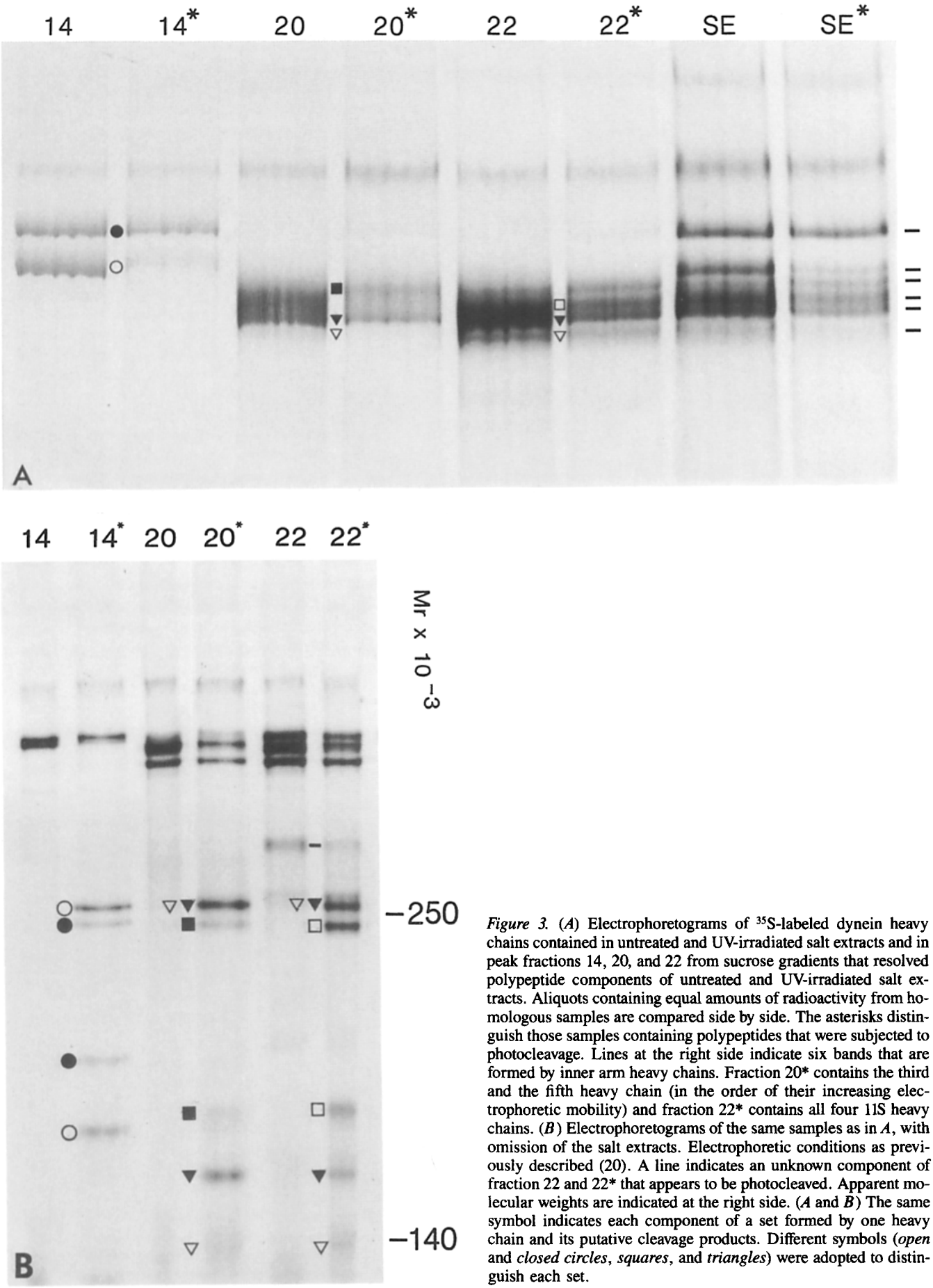

Figure 3. (*A*) Electrophoretograms of ^{35}S-labeled dynein heavy chains contained in untreated and UV-irradiated salt extracts and in peak fractions 14, 20, and 22 from sucrose gradients that resolved polypeptide components of untreated and UV-irradiated salt extracts. Aliquots containing equal amounts of radioactivity from homologous samples are compared side by side. The asterisks distinguish those samples containing polypeptides that were subjected to photocleavage. Lines at the right side indicate six bands that are formed by inner arm heavy chains. Fraction 20* contains the third and the fifth heavy chain (in the order of their increasing electrophoretic mobility) and fraction 22* contains all four 11S heavy chains. (*B*) Electrophoretograms of the same samples as in *A*, with omission of the salt extracts. Electrophoretic conditions as previously described (20). A line indicates an unknown component of fraction 22 and 22* that appears to be photocleaved. Apparent molecular weights are indicated at the right side. (*A* and *B*) The same symbol indicates each component of a set formed by one heavy chain and its putative cleavage products. Different symbols (*open* and *closed circles*, *squares*, and *triangles*) were adopted to distinguish each set.

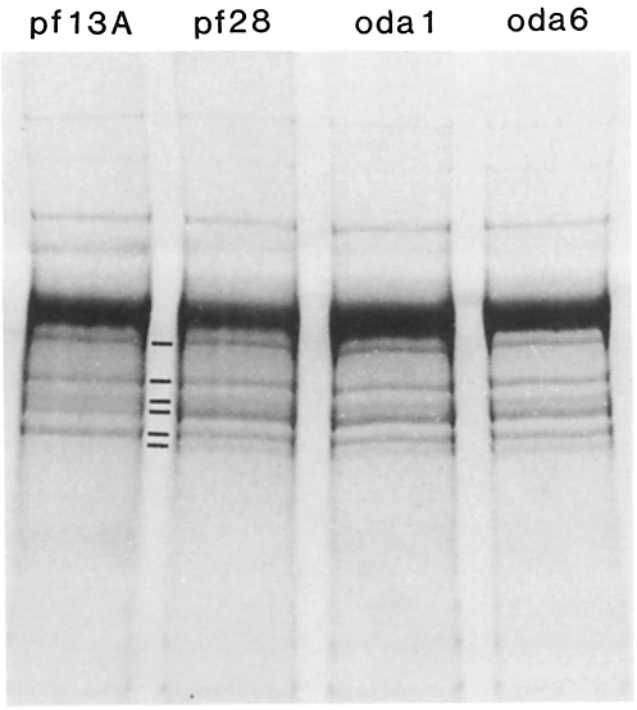

Figure 4. Electrophoretograms of ^{35}S-labeled flagellar polypeptides from outer arm-less mutants *pf*13A, *pf*28, *oda*1, and *oda*6. Inner dynein arm heavy chains are indicated by lines. Flagella of *pf*13A are paralyzed as opposed to those of *pf*28, *oda*1, and *oda*6, which are motile. The intense, wide band present in each electrophoretogram is a flagellar membrane protein.

Inner Arm Heavy Chains of Motile and Immotile and Short Flagella

The relative intensity of a subset of the electrophoretic bands formed by the inner arm heavy chains changes depending on whether they are derived from axonemes of motile or immotile and short flagella. The outer arm–less mutant *pf*13A has immotile, short flagella in contrast to the outer arm–less mutants *pf*28, *oda*1, and *oda*6, which have motile flagella (15). Fig. 4 shows that the electrophoretic pattern of heavy chains of *pf*13A flagella is different from that of the motile outer arm-less flagella. Only five inner arm heavy chains were resolved for *pf*13A, whereas six inner arm heavy chains were resolved for the other mutants. The upper two bands are equal in intensity in each of the mutants irrespective of motility, whereas the lower three remaining bands in *pf*13A differ in their intensities from each other and from those in *pf*28, *oda*1, and *oda*6. The electrophoretic patterns formed by *pf*28, *oda*1, and *oda*6 heavy chains are indistinguishable.

Quantitative densitometry of electrophoretograms indicates that the sum intensity of the lower three bands of *pf*13A is very close to that of the four lower bands in *pf*28, *oda*1, and *oda*6 after normalization toward the upper two bands (data not shown). Therefore, a form of posttranslational modification may result in changes of mobility of heavy chain polypeptides. These changes may be related to the motility and/or the length of the flagella under analysis. Alternatively, a subset of inner arm heavy chains including those forming the two upper bands and two lower bands is absent in immotile and short flagella.

To further test these hypotheses we analyzed flagella and axonemes of the recombinant strains *pf*14*pf*28 and *pf*18-*pf*28, because mutations at the *PF*14 or *PF*18 locus are correlated with drastic reduction of flagellar movement. In addition the recombinant *pf*14*pf*28 and *pf*18*pf*28 have short flagella. The electrophoretograms of the heavy chains of the recombinants (Fig. 5) are very similar to that of the mutant *pf*13A (Fig. 4). Therefore, the relative intensity of the three lower bands formed by inner arm heavy chains changes in correlation with the motility and the length of the flagella under investigation. Furthermore, these experiments show that the five heavy chains of *pf*13A and the recombinant strains are indeed derived from inner dynein arms, and are not located in the radial spokes or central complex of the axoneme because *pf*14 and *pf*18 axonemes lack the radial spokes and the central complex, respectively.

The results of these experiments suggest that a subset of the six inner arm heavy chains is differentially modified or absent in motile or immotile and short flagella. Additional data from other immotile and short inner arm mutants (discussed below) are also consistent with these results. However, these results do not resolve the issue of whether the 11S heavy chains form one or two kinds of inner dynein arms of distinct location within the axoneme. To address this question, we used electrophoretic and electron microscopic analyses of inner arm components in inner arm defective mutants.

Inner Arm Mutants Lacking Different Subsets of Heavy Chains

The investigation concerned with the heterogeneity of the inner dynein arms was continued with the analysis of the mutants *pf*23 and *pf*30 because previous studies had revealed that these mutants are partially defective for inner arm structures and inner arm heavy chains (4, 11, 20).

The mutants *pf*30 and *pf*23 have normal outer dynein arms. Therefore, we isolated and analyzed recombinant strains *pf*30*pf*28 and *pf*23*pf*28 to eliminate the interference of outer arm heavy chains in the electrophoretic resolution

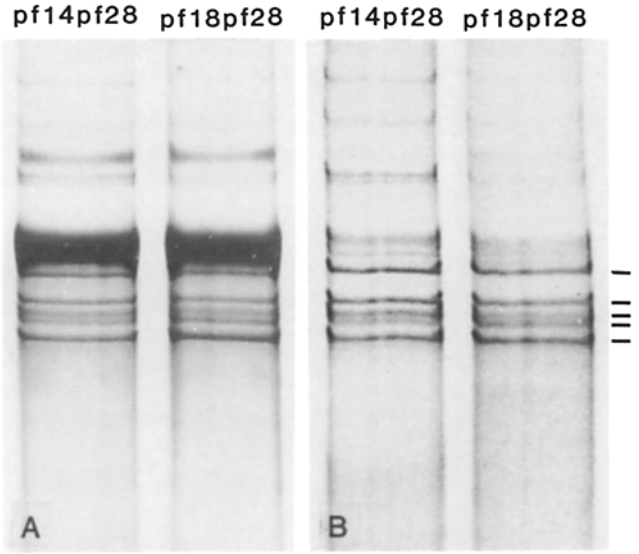

Figure 5. Electrophoretograms of ^{35}S-labeled flagellar (*A*) and axonemal (*B*) polypeptides from recombinant strains *pf*14*pf*28 and *pf*18*pf*28. Inner dynein arm heavy chains are indicated by lines at the right side.

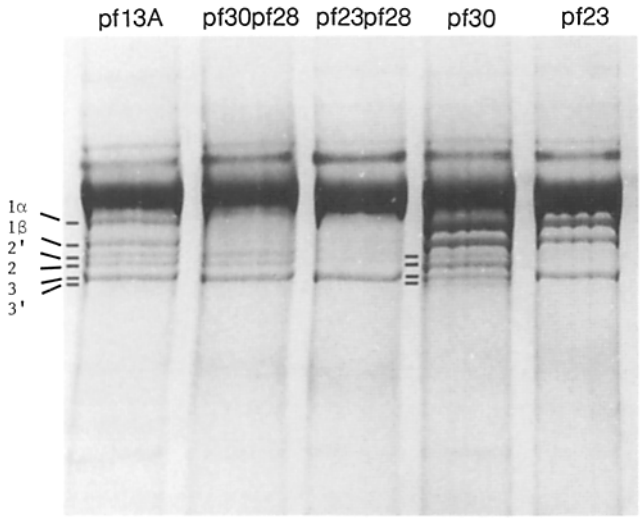

Figure 6. Electrophoretograms of ^{35}S-labeled flagellar polypeptides of the mutant *pf*13A, the recombinant strains *pf*30*pf*28 and *pf*23*pf*28 and the mutant *pf*30 and *pf*23. Equal amounts of radioactivity were analyzed in each lane. Bands referred to as 1α, 1β 2', 2, 3, and 3' are indicated at the left side.

of inner arm heavy chains. We analyzed recombinant strains *pf*30*pf*28 and *pf*23*pf*28, which both have immotile and short flagella, by electrophoresis and compared them with the immotile and short outer arm-less mutant *pf*13A (Fig. 6). The mutants *pf*30 and *pf*23 were included as additional standards. These mutants have motile and normal in length flagella and immotile and short flagella, respectively. Flagella, instead of axonemes, were adopted for the analysis to avoid potential losses of dynein arms during the isolation.

Electrophoretic patterns formed by inner arm heavy chains (Fig. 6), reveal that the recombinant strain *pf*30*pf*28 lacks the components here referred to as 1α and 1β. In contrast, the mutant *pf*30 produces a pattern of six bands indistinguishable from that of wild-type axonemes (compare Figs. 1 and 6), because the outer arm heavy chains are not resolved from 1α and 1β. The four lower bands of the mutant *pf*30, here are referred to as 2', 2, 3, and 3'. Compared with *pf*13A, the recombinant strain *pf*23*pf*28 shows the presence of only component 3, and lacks components 1α, 1β, 2', and 2. The mutant *pf*23 shows the absence of components 2' and 2 and is partially defective for the outer arm heavy chains. In *pf*13A and *pf*30*pf*28, component 3 forms a more intense band than those of component 2 and 2'.

This evidence shows that the inner arm defective strains *pf*30 and *pf*23 are defective for a set of two and for a set of four inner arm heavy chains, respectively. In addition, it confirms that the electrophoretic patterns of heavy chains, other than 1α and 1β, change depending on the motility and/or length of the flagella under investigation. These results suggest there are three types of inner arm components in ~1:1:1 ratio, each composed of a different set of two heavy chain subunits. To further test this idea we examined the same inner arm defective mutants, and recombinant strains, by EM to look for gaps in the row of inner arm structures.

Electron Microscopy in Mutants Lacking Different Subsets of Inner Arm Heavy Chains

The existence of three distinct inner arm structures was confirmed by EM of longitudinal sections of axonemes from the mutants *pf*30 and *pf*23. Two section planes, *A* and *B* as illustrated in Fig. 7, were chosen for analysis. Section A bisects the axoneme since most or all of the central complex is seen (Fig. 8, *left*). The S1 and S2 radial spokes are viewed in their entirety in such sections. Section B is a glancing section that does not include the central complex and in which the radial spokes are viewed in cross section or end on (Fig. 8, *right*). In both section types the proximally directed tilt of the outer arms (10) is seen in wild-type, *pf*30, and *pf*23 axonemes and permitted determination of the orientation of the axoneme: the proximal end is to the left in Fig. 8. Interpretative tracings are included beneath each micrograph.

Both A and B sections of wild-type axonemes show the row of inner dynein arms as a nearly continuous ribbon of electron opaque material but occasionally interrupted by indentations or small spaces, indicated by vertical lines and arrows in Fig. 8, that repeat between spoke group pairs with a 96-nm period. The indentation or space between groups of inner arms appears to be the same defined in other structural studies using quick freeze and rotary shadow methods (for discussion see reference 8). The inner row of dynein arms is thus likely to be formed by groups of structures repeating with the same periodicity as the paired spokes (7, 8). Additional microscopic images of *pf*14*pf*28 and *pf*18*pf*28 confirmed that the inner row of dynein arms is formed by groups of structures delineated by indentations of specific location between spoke group pairs repeating every 96 nm (data not shown). Therefore, the lack of radial spokes or central components or outer dynein arms does not affect the grouping of inner arm structures resolved by thin sections.

In contrast to axonemes with complete sets of inner dynein heavy chains, similar longitudinal sections of *pf*30 and *pf*23 revealed the existence of obvious and relatively large gaps in the row of inner dynein arms, indicated by arrowheads in Fig. 8. In all cases, gaps and intervening stained inner arms have a repeat of 96 nm in constant position and polarity relative to radial spoke organization. The gaps seen in *pf*30 are located in the large interval defined by the radial spokes just proximal to spoke S1, the proximal spoke of each pair, and

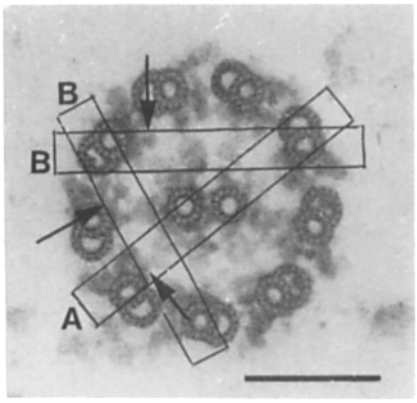

Figure 7. Thin section electron micrograph of a wild-type axoneme illustrating the two types of longitudinal sections shown in Fig. 8. The two orientations are referred to as *A* and *B* sections and here are indicated by lines superimposed on the transverse section. Arrows point towards inner arms contained within each longitudinal section type. Bar, 0.1 μm.

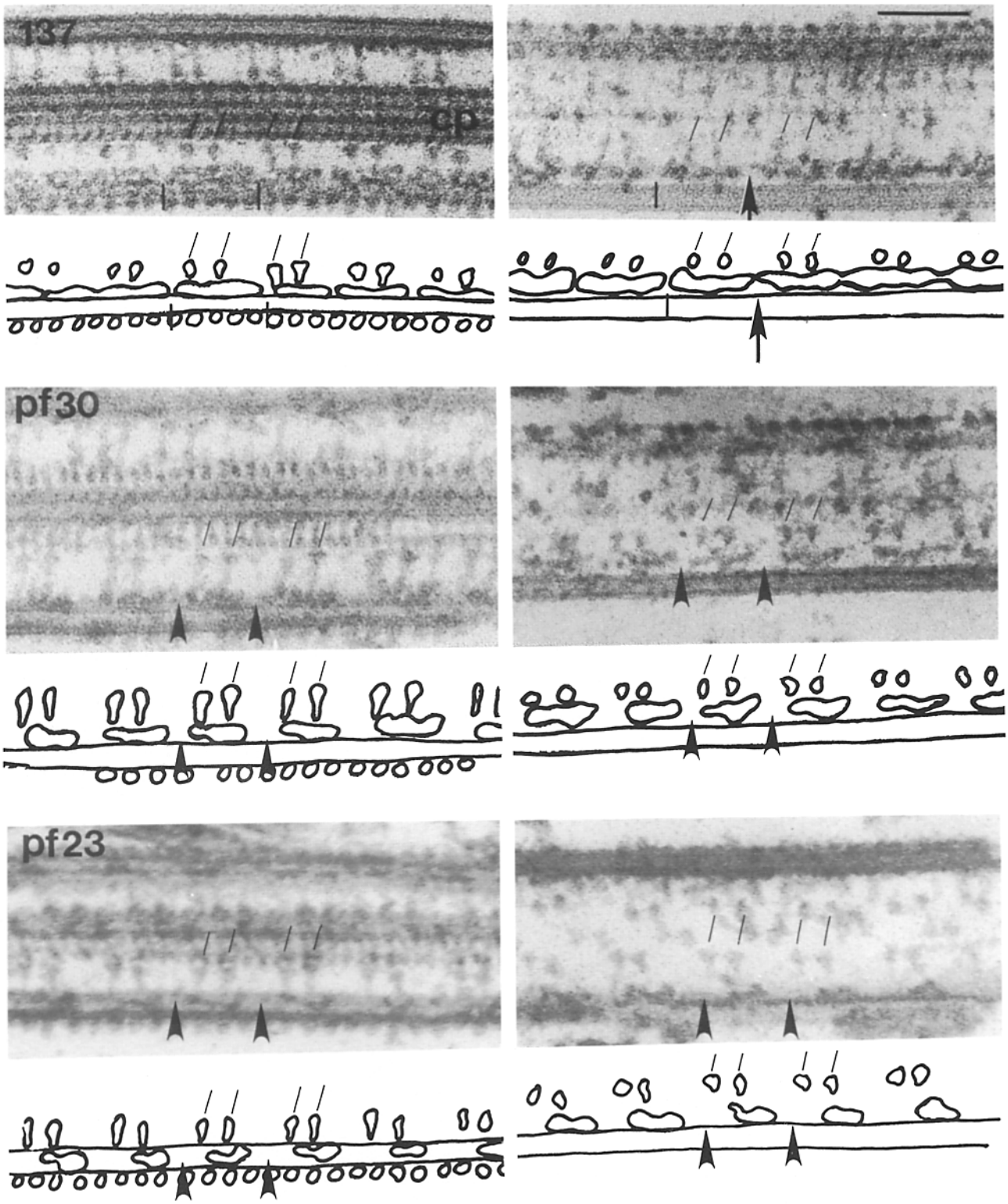

Figure 8. Thin-section micrographs and corresponding interpretive traces of wild-type and mutant axonemes. (*Left* and *right*) *A* and *B* longitudinal sections, respectively, (see Fig. 7 for orientation) and from top to bottom contain longitudinal sections and traces of wild-type (137), *pf*30, and *pf*23 axonemes. The proximal ends of the axonemes are oriented to the left. Oblique lines indicate radial spokes. Vertical lines in wild-type axonemes indicate identations or spaces that ordinarily define 96-nm repeats of inner arm groups. However, the wild-type A image selected contains one indentation of atypical position (*right-most vertical line*) and the wild-type B image selected contains an unusually wide space (arrow, see text for discussion). In axonemes from mutant cells, gaps in inner arm structure are indicated by arrowheads. Gap size (see Results) was measured between clearly distinguishable electron dense structure of the remaining inner arms. For example, the left arrowhead in the *pf*30 A image indicates a gap which would not have been included for measurement since its boundaries are not obvious (frequency of measurable gaps is described in Results). CP, the central pair in the wild-type A section; bar, 0.1 μm.

comprise approximately one-third the length of the 96 nm repeat (37 ± 8 nm, $n = 30$: for criteria used to measure gaps see legend to Fig. 8). Gaps of the same size (37 ± 8 nm, $n = 30$) and location were also seen in sections of the recombinant mutant *pf*30*pf*28, indicating that the lack of outer arms does not affect the spacing of the inner arms. Moreover, in an independent study of *pf*30 using quick-freeze, rotary shadow replication, a gap was also found just proximal to each radial spoke S1 (Goodenough, U. W., personal communication).

Occasionally gaps of similar size and disposition as in *pf*30 axonemes were found in wild-type axonemes (Fig. 8, *top right*, indicated by *arrow*). In order to evaluate the significance of that morphological variation we determined gap frequency for 34 consecutive spoke group repeats >3.0 μm of randomly selected, longitudinally sectioned axonemes from wild-type and *pf*30. Four gaps, ~25 nm wide, were identified in wild-type axonemes. In contrast 28 gaps, ~35 nm wide, were identified in *pf*30. Therefore, the origin of the gaps observed in wild-type axonemes is different from that of the gaps found in *pf*30 axonemes.

Regular repeating gaps were also found in *pf*23 inner arms. These gaps were much larger spanning about two-thirds of the 96-nm spoke repeat interval (67.9 ± 5 nm, $n = 31$) and encompassed the gap found in *pf*30. In an analysis similar to that described above, 30 gaps, ~65 nm wide, were found in 34 consecutive spoke repeats >3.0 μm of randomly selected axonemes from *pf*23 cells. The remaining inner arm structure of *pf*23 axonemes was found under and just distal to S2.

These combined structural and biochemical analyses of inner arm defective mutants indicate that a pair of inner arm heavy chains, 1α and 1β, is missing in *pf*30 and correlate this deficiency with the gap making up approximately one-third of the 96-nm arm repeat. Four heavy chains, 1α, 1β, 2′, and 2, are missing in *pf*23 and this correlates with a gap about two-thirds the length of the 96-nm repeat. These results are consistent with a model in which components 1α and 1β form an inner arm located proximal to spoke S1, referred to as inner arm I1, and components 2′ and 2 form an inner arm structure located proximal to S2, referred to as I2. Therefore, a third inner arm, I3, located at the base and distal of the spoke S2 would be composed of heavy chains 3 and 3′.

Discussion

The Organization of the Row of the Inner Dynein Arms

The evidence described in the preceding section has revealed the following aspects of the molecular composition and the organization of the inner dynein arms row. First, the inner arms can be distinguished as three different structures that are located in precise positions relative to the radial spokes. Second, each inner arm structure is composed of two heavy chains each having a site for ATP hydrolysis. Finally, the inner arms I2 and I3 were found to be more similar to each other than to the inner arm I1. These new insights were obtained by an electrophoretic procedure resolving the inner arm heavy chains into six components and by electron microscopy of longitudinal sections of wild-type and mutant axonemes. In addition, recombinant strains carrying the *pf*28 mutation (lacking the outer dynein arms) were constructed and analyzed whenever outer arm heavy chains interfered with the resolution of inner arm heavy chains.

On the basis of this new evidence, the row of inner dynein arms appears to be formed by three distinct inner arms that are organized in groups of three and repeat at 96 nm. This model is in agreement with the models of inner dynein arm organization proposed by Goodenough and Heuser (7, 9) which were derived from quick-freeze, rotary shadow, structural analyses of unfixed axonemes. Goodenough and Heuser described two morphologically distinct inner arm types: one termed a triad and the other termed a dyad. The triads and dyads alternate every 96 nm along each doublet microtubule in sets formed by one triad and two dyads. Based upon the position relative to the spokes we conclude that I1 is identical to what was termed a triad and I2 and I3 are the proximal and distal dyads, respectively. Our results are inconsistent with other models in which inner and outer rows of arms are thought to be identical in organization (2).

The triad (I1) was originally defined based upon the observation, in metal replicas, that it contained three large globular heads as opposed to the two heads in each dyad (7). To date, all dyneins have been shown to contain equal numbers of heavy chains and globular heads (28). Because the evidence described in this paper suggests that inner I1, the triad, is formed by two heavy chains, it would appear that the triad is an exception. However, the most recent description of inner arm images obtained by quick-freeze, deep-etch microscopy (8) redefine the triad as composed of a bilobed unit adjacent to a two-headed structure similar to a dyad. Therefore, a third globular domain of the triad, perhaps the bilobed structure, may not be composed of one of the inner arm heavy chains.

On the basis of our present understanding of the organization of the row of inner and outer dynein arms we can explain some results obtained in the past. Both mutants *pf*23 and *pf*30 were found to be defective for inner dynein arm structures by examination of cross-sectional images of isolated axonemes (4, 11). We understand now that the absence or the reduction in intensity seen among the inner arm structures resulted from the lack of the inner arm I1 and I2 in *pf*23 and I1 in *pf*30. In fact, those defects were observed in cross sections of thickness close to the dimension of the periodic repeat of each inner dynein arm (for discussion see reference 4).

In the past, the resolution of outer and inner dynein arm heavy chains from *Chlamydomonas* wild-type and dynein arm defective mutants, suggested the existence of three outer and five inner dynein arm heavy chains that could be distinguished by the intensity of the electrophoretic bands formed by each of them (17). The bands of outer arm components were much more intense than those of inner arm components whereas components of each group were similar to each other. We presently know that within a 96-nm segment of outer doublet microtubules there are four outer dynein arms (9, 11) and three inner dynein arms, respectively, composed of three and two heavy chains each. Therefore, the molar ratio of outer versus inner arm heavy chains is 2:1 in agreement with what was observed earlier (11). Similarly, with respect to the inner arm heavy chain stoichiometry, Mitchell and Rosenbaum (19) describe four inner arm heavy chains in *pf*28 in an apparent ratio 1:1:2:2. Those data are consistent with our identification of six inner arm heavy chains.

Molecular Composition of Each Inner Arm

The following properties clearly distinguish the inner arm I1 from the inner arms I2 and I3. I1 is formed by at least three polypeptides that have distinctive electrophoretic mobility and are not dissociated upon sucrose gradient centrifugation at high ionic strength. In contrast, both I2 and I3 may be formed by the same group of light chains and are dissociated into 11S particles at high ionic strength. Further, I1 has a distinct "triad" structure compared to the dyad structure of I2 and I3 when studied in situ by the quick-freeze, rotary shadow method (8). Therefore, I1 is quite different from I2 and I3, and these last two are similar.

We could distinguish between the inner arms I2 and I3 by analyzing the mutant *pf*23 and the recombinant strain *pf*23-*pf*28, because inner arm heavy chains 2′ and 2 were lacking in the flagella of those strains in addition to the heavy chains 1α and 1β. That deficiency could derive from the absence of the subunits composing the inner arm I2 or from the defect in a putative mechanism of posttranslational modification converting the heavy chain 3 into 2′ and 2. However, this second event appeared unlikely because flagella of the strain *pf*23*pf*28 do not have a greater amount of heavy chain 3 than the flagella of *pf*30*pf*28, which have inner arm I2. Therefore, the heavy chains 3 and 2′ and 2 are not in a precursor–product relationship and the inner arm I2 is distinct from I3. The EM analyses confirmed this point.

Posttranslational modifications converting the inner arm heavy chain 2 into heavy chain 2′ and 3 into 3′ may exist because the stoichiometry between the components of the two sets is altered in mutants carrying immotile and short flagella. Moreover, at least two of those heavy chains are phosphorylated in vivo (24). On this basis each of the inner arms I2 and I3 may be formed by two heavy chains that are identical in their amino acid sequence. On the other hand, there is no direct evidence that posttranslational modifications account for the differences in electrophoretic mobility of the heavy chains 2′, 2, or 3, and 3′. Alternatively, the differences in the electrophoretic patterns of inner arm heavy chains that were observed when mutants with motile flagella were compared to mutants with immotile and short flagella could derive from a partial loss of components 1α, 1β, 2, and 3′.

A form of actin is one of the light chains forming the inner arms I2 and I3 (23). In addition, the 19,000-molecular weight protein, cosedimenting with the actin in the 11S particles derived from I2 and I3, appeared to be identical to the calcium-binding protein caltractin which was initially identified as a *Chlamydomonas* basal body component (14). Caltractin is also similar or identical to centrin (14, 26). We have confirmed the identity of the 19,000 molecular weight protein and caltractin by electrophoresis and immunoblots of the polypeptides forming the 11S complexes from the inner arms. A polyclonal antibody to caltractin (14) (kindly provided by Dr. Bessie Huang, Research Institute of Scripps Clinic, La Jolla, CA) bound uniquely to the 19,000-molecular weight component (Piperno, G., unpublished observation). On this basis the inner arms I2 and I3 contain components that differentiate them from I1 and may regulate their function.

A previous study showed that substoichiometric amounts of actin were found in 11S fractions of 1α and 1β heavy chains that were isolated by subsequent dialysis and sedimentation at low ionic strength (20). However, the association of actin with the I1 heavy chain may be adventitious in light of the observations described above and in the article of Goodenough et al. (9). The isolation of an actin-containing complex at low ionic strength, as was performed in the first study (20), probably was due to nonspecific binding of actin to the I1 heavy chains.

The Regulation of Motility by Inner Arm Components

The phenotypes of the mutants *pf*23 and *pf*30 indicate that the inner dynein arms regulate the movement of *Chlamydomonas* flagella in at least two ways depending on which inner arm is involved.

The lack of the inner arm heavy chains 1α and 1β in flagella of the mutant *pf*30 was correlated with a slight decrease of flagellar beat frequency and a remarkable change in flagellar bending pattern (4). On this basis the inner dynein arms were identified as structures influencing axonemal waveforms and microtubule sliding rate more than the beat frequency although only one specific inner dynein arm I1, was missing.

The mutant *pf*23 was found to lack ~15% of outer dynein arms and 86% of inner dynein arms by examination of cross-sectional images of isolated axoneme (11). We presently know that the mutant *pf*23 lacks the inner arms I1 and I2 but retains the inner arm I3 and most of outer dynein arms. Therefore as a result of our present analysis, the mutants *pf*23 and *pf*30 appear to differ mainly for the additional lack of inner arm I2 in the mutant *pf*23. This lack is correlated with the paralysis of *pf*23, although it does not involve a marked reduction in the number of outer and inner dynein arm heavy chains per unit length of the axoneme relative to that contained in *pf*30. Therefore, the defect of I2 apparently results in a greater inhibition of axonemal movement than would be predicted simply on the basis of the number of remaining dynein arms.

The possible involvement of the inner dynein arms I2 and I3 in a mechanism of regulation of axoneme motility is suggested by the following observations. The mutants lacking all or part of the radial spokes have nonmotile flagella, although they are normal in their outer and inner dynein arm structures (12). However, the same mutations in recombinant strains also carrying $sup_{pf}3$ or $sup_{pf}4$ or *pf*2 and *pf*3, allow for flagellar motility (13). The mutants *pf*2 and *pf*3 have the motility phenotype of inner arm–deficient mutants as does *pf*30 (4). In addition, they are deficient for the phosphorylation of at least one of the inner arm heavy chains forming the I2 and I3 structures (17). Therefore, that specific deficiency of the I2 and I3 inner arm heavy chains is correlated with the suppression of flagellar paralysis.

Additional lines of evidence implicate the inner arms I2 and I3 as structures involved in the regulation of flagellar motility. First, inner arm heavy chains, other than 1α and 1β lacking in *pf*30, are phosphorylated in vivo by pulse ^{32}P-labeling (24). Second, axonemal actin is a subunit of the complexes formed by I2 and I3 heavy chains. Finally, the 19,000-molecular weight protein cosedimenting with actin appears to be identical to the calcium-binding protein caltractin (14). Therefore, inner arms I2 and I3 display features that are involved in the regulation of other contractile sys-

tems: actin, a calcium-binding protein, and the phosphorylation of subunits carrying ATPase activity.

In summary, we have identified some of the molecular components of the three inner dynein arms and revealed that the inner arm proximal to the S1 radial spoke, I1, is different in structure and function from the other two, I2 and I3, both located distal to a radial spoke. The inner arms I2 and I3 from their location in the axoneme may regulate both the radial spoke–central pair interactions (27) and the Ca^{2+}-dependent switching from a ciliary to a flagellar form of motion (3).

Anna Gajewski, Jenifer Nesin, Eleana Sphicas, and Laura A. Fox are acknowledged for their careful technical assistance.

This work was supported by grants GM-17132 (G. Piperno) and HD-00553 and HD-20497 (W. S. Sale) from the National Institutes of Health.

Received for publication 31 July 1989 and in revised form 13 October 1989.

References

1. Adams, G. M. W., B. Huang, G. Piperno, and D. J. L. Luck. 1981. Central-pair microtubular complex of *Chlamydomonas* flagella: polypeptide composition as revealed by analysis of mutants. *J. Cell Biol.* 91:69–76.
2. Avolio, J., A. N. Glazzard, M. E. J. Holwill, and P. Satir. 1986. Structures attached to doublet microtubules of cilia: computer modeling of thin-section and negative-stain stereo images. *Proc. Natl. Acad. Sci. USA.* 83:4804–4808.
3. Bessen, M., R. B. Fay, and G. B. Witman. 1980. Calcium control of waveform in isolated flagellar axonemes of *Chlamydomonas*. *J. Cell Biol.* 86:446–455.
4. Brokaw, C. J., and R. Kamiya. 1987. Bending patterns of *Chlamydomonas* flagella: IV. Mutants with defects in inner and outer dynein arms indicate differences in dynein arm function. *Cell Motil. Cytoskel.* 8:68–75.
5. Gibbons, B. H., and I. R. Gibbons. 1987. Vanadate-sensitized cleavage of dynein heavy chains by 365-nm irradiation of demembranated sperm flagella and its effect on the flagellar motility. *J. Biol. Chem.* 262:8354–8359.
6. Gibbons, I. R. 1989. Microtubule-based motility: an overview of a fast-moving field. *In* Cell Movement. Vol. 1. Alan R. Liss, Inc., NY. 3–22.
7. Goodenough, U. W., and J. E. Heuser. 1985. Substructure of inner dynein arms, radial spokes, and the central pair/projection complex of cilia and flagella. *J. Cell Biol.* 100:2008–2018.
8. Goodenough, U. W., and J. E. Heuser. 1989. Structure of the soluble and *in situ* ciliary dyneins visualized by quick-freeze deep-etch microscopy. *In* Cell Movement. Vol. 1. Alan R. Liss, Inc., NY. 121–140.
9. Goodenough, U. W., B. Gebhart, V. Mermall, D. R. Mitchell, and J.E. Heuser. 1987. High-pressure liquid chromatography fractionation of *Chlamydomonas* dynein extracts and characterization of inner-arm dynein subunits. *J. Mol. Biol.* 194:481–494.
10. Haimo, L. T., B. R. Telzer, and J. L. Rosenbaum. 1979. Dynein binds to and crossbridges cytoplasmic microtubules. *Proc. Natl. Acad. Sci. USA.* 76:5759–5763.
11. Huang, B., G. Piperno, and D. J. L. Luck. 1979. Paralyzed flagella mutants of *Chlamydomonas reinhardtii*. *J. Biol. Chem.* 254:3091–3099.
12. Huang, B., G. Piperno, Z. Ramanis, and D. J. L. Luck. 1981. Radial spokes of *Chlamydomonas* flagella: genetic analysis of assembly and function. *J. Cell Biol.* 88:80–88.
13. Huang, B., Z. Ramanis, and D. J. L. Luck. 1982. Suppressor mutations in *Chlamydomonas* reveal a regulatory mechanism for flagellar function. *Cell.* 28:115–124.
14. Huang, B., D. M. Watterson, V. D. Lee, and M. J. Schibler. 1988. Purification and characterization of a basal body-associated Ca^{2+}-binding protein. *J. Cell Biol.* 107:121–131.
15. Kamiya, R. 1988. Mutations at twelve independent loci result in absence of outer dynein arms in *Chlamydomonas reinhardtii*. *J. Cell Biol.* 107: 2253–2258.
16. Kamiya, R., E. Kurimoto, H. Sakakibara, and T. Okagaki. 1989. A genetic approach to the function of inner and outer arm dynein. *In* Cell Movement. Vol. 1. Alan R. Liss, Inc., NY. 209–218.
17. Luck, D. J. L., and G. Piperno. 1989. Dynein arm mutants of *Chlamydomonas*. *In* Cell Movement. Vol. 1. Alan R. Liss, Inc., NY. 49–60.
18. Luck, D. J. L., G, Piperno, Z. Ramanis, and B. Huang. 1977. Flagellar mutants of *Chlamydomonas*: studies of radial spoke-defective strains by dikaryon and revertant analysis. *Proc. Natl. Acad. Sci. USA.* 74:3456–3460.
19. Mitchell, D. R., and J. L. Rosenbaum. 1985. A motile *Chlamydomonas* flagellar mutant that lacks outer dynein arms. *J. Cell Biol.* 100:1228–1234.
20. Piperno, G. 1988. Isolation of a sixth dynein subunit adenosine triphosphatase of *Chlamydomonas* axonemes. *J. Cell Biol.* 106:133–140.
21. Piperno, G., and D. J. L. Luck. 1976. Phosphorylation of axonemal proteins in *Chlamydomonas reinhardtii*. *J. Biol. Chem.* 251:2161–2167.
22. Piperno, G., and D. J. L. Luck. 1979. Axonemal adenosine triphosphatases from flagella of *Chlamydomonas reinhardtii*. *J. Biol. Chem.* 254:3084–3090.
23. Piperno, G., and D. J. L. Luck. 1979. An actin-like protein is a component of axonemes from *Chlamydomonas* flagella. *J. Biol. Chem.* 254:2187–2190.
24. Piperno, G., and D. J. L. Luck. 1981. Inner arm dyneins from flagella of *Chlamydomonas reinhardtii*. *Cell.* 27:331–340.
25. Sale, W. S., L. A. Fox, and S. L. Milgram. 1989. Composition and organization of the inner row dynein arms. *In* Cell Movement. Vol. 1. Alan R. Liss, Inc., NY. 89–102.
26. Salisbury, J. L., A. T. Baron, and M. A. Sanders. 1988. The centrin-based cytoskeleton of *Chlamydomonas reinhardtii*: distribution in interphase and mitotic cells. *J. Cell Biol.* 107:635–641.
27. Warner, F. D., and P. Satir. 1974. The structural basis of ciliary bend formation. Radial spoke positional changes accompanying microtubule sliding. *J. Cell Biol.* 63:35–63.
28. Witman, G. B. 1989. Composition and molecular organization of the dyneins. *In* Cell Movement. Vol. 1. Alan R. Liss, Inc., NY. 25–35.
29. Witman, G. B., J. Plummer, and G. Sander. 1978. *Chlamydomonas* flagellar mutants lacking radial spokes and central tubules. *J. Cell Biol.* 76:729–747.